JOURNAL OF PROPULSION AND POWER
Vol. 23, No. 6, November–December 2007

Experimental Study of a Combined-Cycle Engine Combustor in Ejector-Jet Mode

Takeshi Kanda,* Kanenori Kato,† Kouichiro Tani,‡ Kenji Kudo,§ and Atsuo Murakami§
Japan Aerospace Exploration Agency, Kakuda, Miyagi 981-1525, Japan

DOI: 10.2514/1.29789

A combustor model of a rocket–ramjet combined-cycle engine was tested in the ejector-jet mode under a sea-level, still condition. The model had two rockets in the duct. Propellants were gaseous hydrogen and oxygen. Design factors of the combustor were cross sections at the entrance and the exit, length of the combustor, fuel injection position, and rocket operating conditions. In the tests, the designed operation of the ejector jet was successfully attained, that is, breathed air was choked at the throat section. Supersonic rocket exhaust and air were decelerated in the divergent duct with an increase of the wall pressure. Fuel was injected in the downstream straight section and combustion gas choked at the exit. The mean Mach number was unity, and the mean combustion efficiency was 0.8 according to the pitot pressure measurement and gas sampling. Suction performance was increased with an increase of the mixture ratio of the rockets. The pressure level in the model was affected by the length of the upstream straight section. The combustion status was not affected by the length of the downstream straight section or the position of fuel injection. An increase of fuel caused an increase of the pressure until attainment of a stoicheometric condition.

Nomenclature

A	=	cross section
CRe	=	contraction ratio of downstream straight section area to exit throat
CRi	=	contraction ratio of width of upstream throat section to width of throat section
c^*	=	characteristic exhaust velocity
D	=	diameter
$h2$	=	height of combustor at exit
$L1$	=	length of upstream straight section
$L2$	=	length of downstream straight section
M	=	Mach number
$\dot{m}$	=	mass flow rate
O/F	=	mixture ratio of oxidizer mass flow rate to fuel mass flow rate
P	=	pressure
T	=	temperature
$w1$	=	width of combustor at entrance
x	=	streamwise distance from rocket nozzle exit position
$\phi 2$	=	total equivalence ratio of fuel injected in downstream straight section

Subscripts

a	=	air
c	=	combustion gas, combustion chamber
mx	=	mixture
r	=	rocket
w	=	wall

Presented as Paper 0223 at the 44th Aerospace Sciences Meeting and Exhibit, Reno, NV, 9–12 January 2006; received 15 January 2007; revision received 17 May 2007; accepted for publication 13 July 2007.

*Manager, Combined Propulsion Research Group, 1 Koganesawa, Kimigaya; kanda.takeshi@jaxa.jp. Senior Member AIAA.

†Senior Researcher, Combined Engine System Section, Combined Propulsion Research Group, 1 Koganesawa, Kimigaya; kato.kaennori@jaxa.jp. Member AIAA.

‡Leader, Combined Engine System Section, Combined Propulsion Research Group, 1 Koganesawa, Kimigaya; tani.kouichiro@jaxa.jp. Member AIAA.

§Senior Researcher, Combined Engine System Section, Combined Propulsion Research Group, 1 Koganesawa, Kimigaya.

I. Introduction

COMBINED-CYCLE engines have been studied for application in aerospace planes and hypersonic flight vehicles. A rocket–ramjet combined-cycle engine, namely, a rocket-based combined-cycle engine (RBCC), is one of the engines suitable for such vehicles [1,2]. Figure 1 shows a schematic diagram of the engine. The most famous concept of RBCC is the strutjet [3,4]. Using breathed air, the engine attains a larger specific impulse than the rocket engine. There are several kinds of rocket–ramjet combined-cycle engines with different aerodynamic and combustion conditions. For example, fuel for breathed air is supplied by residual fuel of the rocket exhaust in one system, while it is supplied from a fuel injector downstream of the rocket in another.

The rocket–ramjet combined-cycle engine has been studied [5–13]. In this engine, there is no strut and the rocket engines are installed in the ramp-shaped top wall. The engine is composed of the ejector jet, ramjet, scramjet, and rocket modes. Figure 2 shows a schematic of the operating modes. Fuel for breathed air is supplied from a fuel injector downstream of the rocket in the ejector jet and ramjet modes. In the scramjet mode, the rocket supplies fuel-rich, precombustion gas as fuel. Combustor tests have been conducted in the ramjet mode [10,11]. Scramjet mode combustor tests in a high specific impulse condition have been conducted with a model having two rockets working as precombustion, fuel-rich gas suppliers [12]. Ejector-jet tests have also been conducted [13–15]. In the tests with engine models, rocket exhaust was simulated with nitrogen gas and engine operation was demonstrated [14,15].

In the present paper, experimental results of a combustor model in the ejector-jet mode are presented. Demonstration of the ejector-jet mode operation of the combustor was the primary objective of the present study, and the method of design of the engine model was also evaluated. Effects of other design factors, for example, length of the combustor, on suction and/or combustion performances were also investigated.

II. Experimental Model

A. Design of Combustor Model

Figure 3 shows the setup of an experimental model of the combustor. Because this combustor model is also to be used for tests in the ramjet and scramjet modes, the entrance geometry was

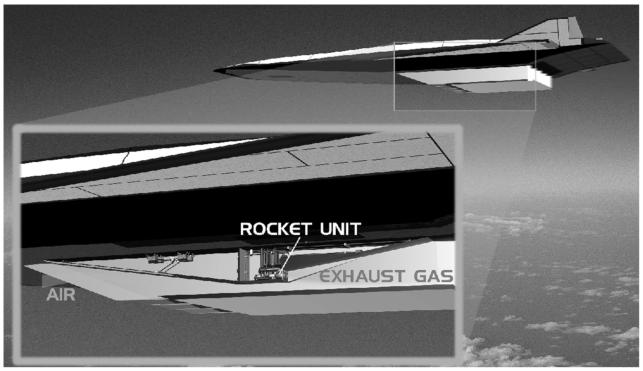

Fig. 1 Schematic of rocket–ramjet combined-cycle engine.

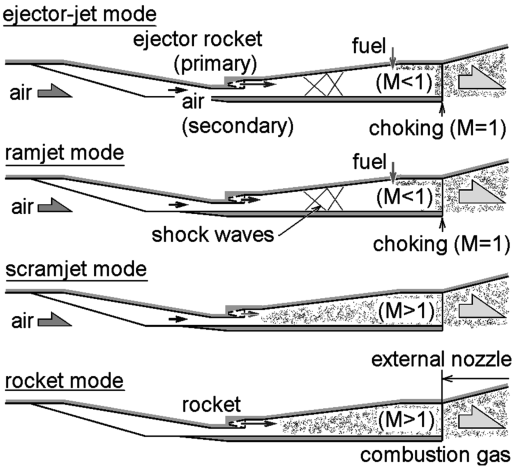

Fig. 2 Schematic of operating conditions of rocket–ramjet combined-cycle engine.

designed so that the combustor could be connected to the M1.7 facility nozzle with a flange. The width can be adjusted by the insertion of auxiliary parts in this ejector-jet mode testing. Operating conditions and the amount of breathed air were estimated with a simple model [5,13]. In this model, momentum is exchanged between the breathed air and the rocket exhaust by the pressure at the dividing streamline. The gases after the exchange were presumed to flow in parallel under the same static pressure, conserving total impulse function, mass, and energy. Base pressure around the rocket nozzles would be much lower than the pressure of the choked airflow or the rocket exhaust. Therefore, the pressure on the base area around the rocket nozzles was presumed to be zero for simplicity. Gases were assumed to be in the equilibrium condition in the calculation.

Propellants were gaseous hydrogen and gaseous oxygen. The rocket chamber pressure and the throat diameter were selected so that air could be breathed into the model under the flow rates of the hydrogen and oxygen gases which the facility could supply. On a rectangular base area, two rocket nozzles were integrated. These geometries resembled that of the engine studied in the conceptual studies [5,6]. Design chamber pressure and mixture ratio of the rockets, $(O/F)_r$, were 2.6 MPa and 8, respectively. The mixture ratio was selected so as to attain the greatest efficiency of combustion of fuel injected into the downstream straight section. The throat and exit diameters of the rocket nozzle were 13 and 18 mm, respectively. The area ratio of the nozzles was small, and the Mach number was 2.0 at the nozzle exit. Pressure at the exit of the rocket nozzles was 370 kPa, larger than atmospheric pressure, due to the rather small area ratio of the nozzles. The nozzles were of conical shape for simplicity of machining, and their divergent angle was 30 deg.

The supersonic airflow and rocket exhaust were presumed to expand isentropically in the divergent section with no mixing upstream of the pseudoshock. The gases decelerated to subsonic

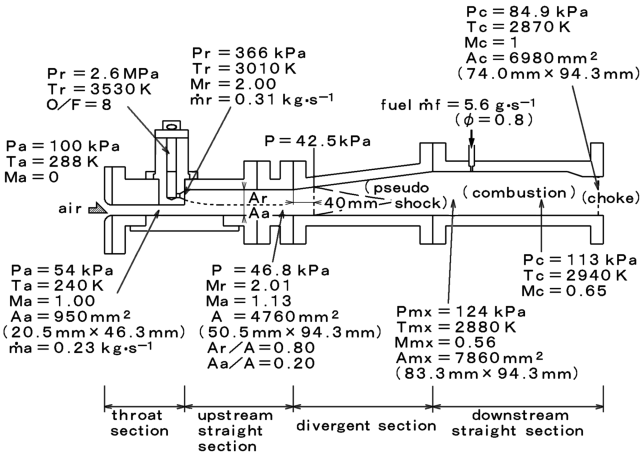

Fig. 3 Calculated operating condition at design condition.

speed and were mixed in the region of the pseudoshock in the section. Both the length of the pseudoshock and the reaction force in the pseudoshock region were estimated with the momentum balance model [9]. Fuel hydrogen for the breathed air was injected into the mixture in the downstream straight section. In the design calculation, combustion efficiency was presumed to be unity. Further combustion accelerated the gas to sonic speed. Geometrical convergence facilitated the acceleration. This choking sustained increased pressure in the downstream straight section. The pressure was determined based on the equivalence ratio of fuel injected into the downstream straight section $\phi 2$ and the exit throat height $h2$. The equivalence ratio was set to be 0.8. Calculated properties at the design condition are listed in Fig. 3.

In the design condition, $w1$ and $h2$ were 46.3 mm and 74.0 mm, respectively. The amount of breathed air was 0.23 $\mathrm{kg \cdot s^{-1}}$. The ratio of the amount of the rocket exhaust to the air was 1.35. The starting position of the pseudoshock was 40 mm downstream of the entrance of the divergent section. Pressure of the mixture in the downstream straight section was 124 kPa, larger than atmospheric pressure. At the same rocket operating condition with no fuel injection in the downstream straight section, the starting position of the pseudoshock was 160 mm downstream of the entrance, and the pressure in the downstream straight section was 108 kPa. The pressure was 16 kPa lower than that with the fuel injection. The effect of the secondary combustion on pressure clearly appears at a higher speed with a larger airflow rate [6].

Heat flux from the combustion gas at the throat was estimated with the method of Bartz [16]. When the rocket chamber pressure was 4 MPa, it was 55 $\mathrm{MW \cdot m^{-2}}$. Cooling water was presumed in the nucleation boiling region. Heat flux to the water was calculated with the equation of Niino et al. [17] and that of Jens and Lottes [17]. Because the calculation results indicated that the rocket chamber could not be cooled to a thermal equilibrium condition, the rocket operating period and the chamber pressure were limited to 5 s and 3 MPa, respectively. This chamber pressure was necessary to keep the pressure at the exit throat around atmospheric pressure.

B. Experimental Model

Figure 4 shows a schematic of the combustor model. Tests were conducted in a sea-level still condition. The model consisted of a rocket block, a throat section, an upstream straight section, a divergent section, and a downstream straight section. The length of the upstream straight section $L1$ was 210 mm in the baseline design condition. In some tests, this section was shortened to 140 mm to investigate the effect of the length downstream of the rockets on the pressure level in the model. The length of the downstream straight section $L2$ was 330 mm in the baseline design condition. A longer straight section of 660 mm, as shown in Fig. 4, was used to investigate the effect of length on combustion. This longer duct had two fuel injectors and the effect of the fuel injection position on combustion was investigated with this duct. The width of the duct at

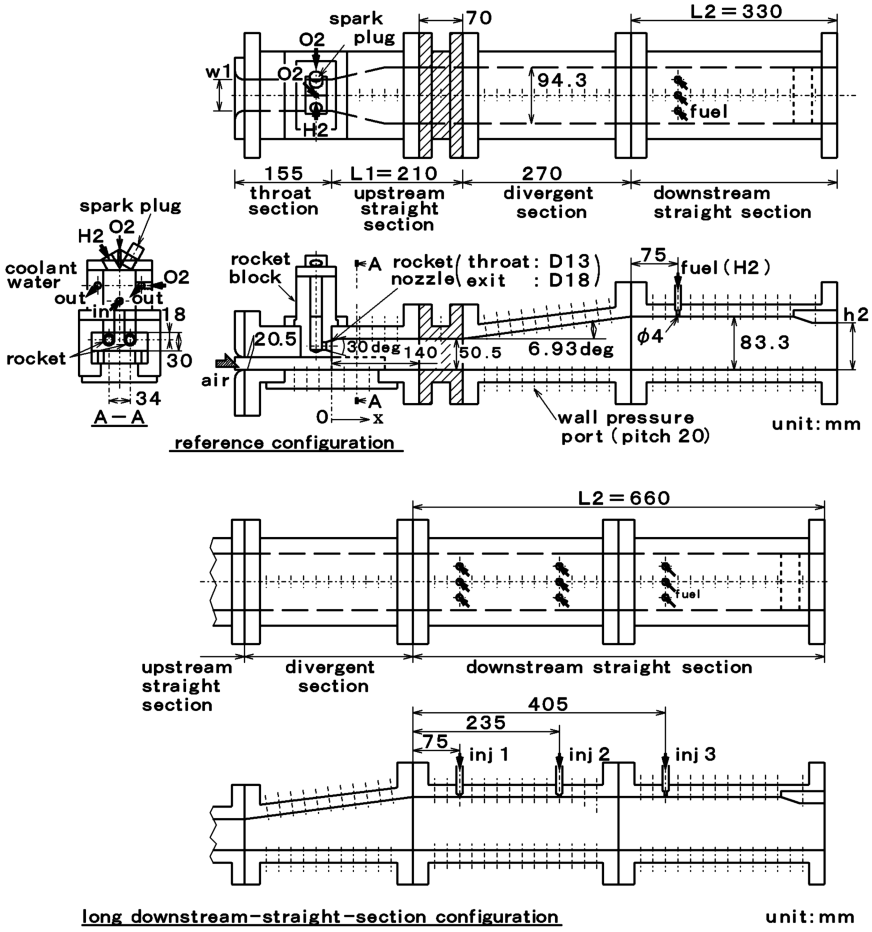

Fig. 4 Schematic of experimental model.

the entrance $w1$ and the height at the exit $h2$ were parameters. The baseline design width and the baseline design height were 46.3 and 74.0 mm, respectively, based on the designed configuration. The width at the model entrance was 94.3 mm with no insertion of blocks. The contraction ratio of the throat section CR_i is defined as the width of 94.3 mm to $w1$, whereas the ratio of the exit throat CR_e is defined as the height of 83.3 mm to $h2$.

The rocket block was made of a copper alloy, and the other sections were made of stainless steel. The rocket combustion chamber was a parallelepiped connected to two rocket nozzles. The standard mixture ratio of the rocket was $(O/F)_r = 8$. c^* efficiency of the rocket was 0.92 with a discharge coefficient of 0.85 [12]. The rocket nozzles were cooled with water. The origin of the x axis was at the exit of the rocket nozzle position as shown in Fig. 4. The wall which had the rocket nozzles is designated as the rocket-side wall, whereas the wall on the other side is the cowl-side wall.

Fuel was injected into the downstream straight section to accelerate the combustion gas for choking at the exit. The equivalence ratio for the fuel was calculated for residual oxygen from the reaction between the breathed air and the rocket exhaust. The amount of breathed air was calculated based on the geometrical cross section at the throat section and measured pressure at $x = 0$ on the cowl-side wall.

C. Measurement

Wall pressure was measured along centerlines on the walls as indicated in Fig. 4. Pressure was measured with a mechanical scanner, SCANIVALVE®, in the 50-ms sampling period. The accuracy of pressure was $\pm 0.2\%$, ± 1.4 kPa in wall and pitot pressure, and ± 10 kPa in rocket chamber pressure. The pressure of the atmosphere was measured with an accuracy of ± 15 Pa.

Pitot pressure measurement and gas sampling [18] were conducted at 60 positions on the exit plane. Sampled gas was analyzed by gas chromatography (Micro-GC CP4900®). The rocket-side wall pressure at the throat was used to calculate gas properties with the measured pitot pressure, in place of static pressure. The combustion efficiency was estimated based on the residual propellants from the rockets and the fuel injected into the downstream straight section. The residual propellants of the rockets were estimated to have a combustion efficiency of 0.8 based on the c^* efficiency. In the estimation process of combustion efficiency, it was presumed that the rocket exhaust and the breathed air were mixed sufficiently in the region of the pseudoshock before the injection of fuel in the downstream straight section. Mean properties were calculated by integration of the local properties. The mass, momentum, and energy were integrated within the measured region. The measured area agreed with the geometrical cross section at the exit of the straight section. Mean molecular weight and specific heats were also calculated. Based on the integrated values and mean gas properties, mean values of combustion efficiency and Mach number were calculated.

III. Results and Discussion

Baseline design conditions were as follows: $w1 = 46.3$ mm $(CRi = 2.04)$, $h2 = 74$ mm $(CRe = 1.13)$, $(O/F)_r = 8$, $P_{c,r} = 2.6$ MPa, and $\phi 2 = 0.8$. According to the model design calculation results, the breathed air would be choked at the entrance, the rocket exhaust and the breathed air would be supersonic at the entrance of the divergent section, and the combustion gas would be choked at the exit. Demonstration of this design operating condition was the primary objective. Design factors, namely, length of the combustor, fuel injection position, areas at the entrance and at the exit, equivalence ratio, and rocket operating conditions, were also investigated in this series of experiments.

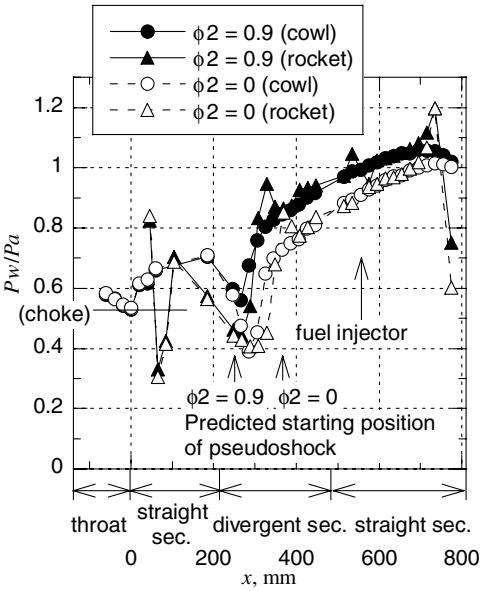

Fig. 5 Wall pressure distributions at baseline design condition.

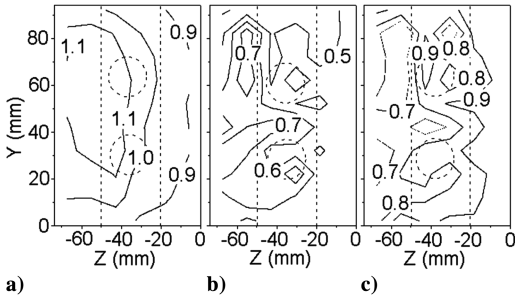

Fig. 6 a) Mach number, b) equivalence ratio, and c) combustion efficiency distributions at the exit at the baseline design condition.

A. Operation at Baseline Design Condition

Figure 5 shows wall pressure distributions at the baseline design condition. The mixture ratio, the pressure of the rocket chamber, and equivalence ratio $\phi 2$ were 8.36, 2.59 MPa, and 0.9, respectively, being slightly different from those of the design condition.

Air was choked at the exit of the throat section. Pressure increased after choking and was higher than the design value. Wall pressure approximately reached the predicted design value around the entrance of the divergent section. The cowl-side wall pressure at the $\phi 2 = 0$ condition became lower than the choking pressure of still air. This decrease of pressure in the divergent section showed that the gases were at supersonic speed. Thus, the downstream flow condition did not affect the pressure distributions upstream of the divergent section at $\phi 2 = 0.9$ and $\phi 2 = 0$. The subsequent increase and recovery of pressure indicated a deceleration of gases. The starting position of the increase of wall pressure, that is, the starting position of the pseudoshock was about 50 mm from the entrance of the divergent section. At the $\phi 2 = 0$ condition, the position was 120 mm. These positions agreed reasonably well with the predicted ones in the design.

The highest pressures in the downstream straight section were lower than the values predicted in the design process. Such deterioration was probably caused by a lower combustion efficiency and a smaller amount of breathed air. The peak pressure on the rocket side at $x = 735$ mm was caused by blockage of the subsonic flow at a compression corner of the exit throat [19].

The pressure decreased toward the exit, which indicated that the combustion occurred at subsonic speed. This is clearly at a higher CR_e condition, as mentioned later. Pressures on the cowl side and on the rocket side differed at the exit. This disagreement in pressures was caused by the asymmetric throat configuration. The cowl-side wall pressure port at the exit was probably still upstream of the sonic line. The combustion gas was choked at the exit throat. This disagreement of pressures at the model exit also appeared in an aerodynamic testing of a combined-cycle engine model with a similar asymmetric throat configuration [15]. According to the pitot pressure measurement shown in the next section, the mean Mach number was unity at the exit plane.

The rocket-side throat pressure was 76 kPa. Though this value was lower than the predicted pressure in the design calculation, the ratio to the pressure in the downstream straight section was 1.4, namely, close to the design ratio. According to separation criteria [20–22], the pressure ratio is around 1.3 at an inflow Mach number slightly above unity. The combustion gas probably flowed out at supersonic speed with shock waves from the edges at the exit of the combustor model.

B. Properties on Exit Plane

Figures 6a–6c show the Mach number, equivalence ratio, and combustion efficiency distributions on the exit plane at the baseline design condition. The cowl-side surface is at $z = 0$ mm. The y axis is in the lateral direction and its origin is on the sidewall. The frame lines of the figures agree with the geometrical throat. Broken lines represent the rocket nozzles and the base area around the nozzles. Hydrogen collected by the probes constituted 73% of the injected fuel.

Injected fuel and combustion efficiency were approximately uniformly distributed. This indicated sufficient mixing of fuel. The mean combustion efficiency was 0.81. The Mach numbers were around unity and the mean Mach number was 1.0. Combustion gas choked at the exit throat.

Momentum was 620 N, pressure force was 530 N, and the impulse function was 1150 N at the exit. This is about 0.9 of the impulse function of 1240 N at the design calculation. This lower impulse function was caused by the combustion efficiency, being lower than unity. When the inflow impulse function is a product of the atmospheric pressure and the cross section at the model exit, it is 700 N. The thrust by the model is estimated to be 450 N. On the other hand, the impulse function of the rockets is 890 N, based on the c^* efficiency of 0.9, and the thrust by the rockets integrated in the combustor model was 190 N, assuming that the inflow impulse function was 700 N. The thrust by the combustor model was augmented by air breathing and subsequent combustion in the integrated engine-model configuration.

The rocket solo thrust was 740 N at sea level with the nozzle exit diameter of 18 mm. It was larger than the thrust of the model. Generally, in the low-speed range, the ejector-jet engine produces a thrust similar to the rocket solo thrust [6].

C. Entrance Area

An effect of the area at the entrance on suction performance was investigated. Wall pressure distributions are shown in Fig. 7. The width at the entrance $w1$ was 54.3 mm, that is, $CR_i = 1.74$, namely, larger than the baseline design condition. The other conditions were the same as those in the baseline design condition. Figure 8 shows wall pressure distributions in the throat section at several contraction ratios at the $\phi 2 = 0$ condition.

In Fig. 7, breathed air was not choked at the exit of the throat section, but the supersonic flow condition was attained around the entrance of the divergent section. In Fig. 8, pressure in the throat section was increased with the decrease of CR_i. In the experiments, choking was unattainable when CR_i was smaller than 1.74. In the design calculation, choking in the upstream throat was unattainable at $w1 = 74.3$ mm, that is, $CR_i = 1.27$.

In Fig. 7, the disagreement in pressure between the cowl side and the rocket side indicated choking of gases at the exit throat. The wall pressure in the divergent section increased when fuel was injected into the downstream straight section. This pressure in the downstream straight section should increase with an increase of the amount of breathed air at a specified equivalence ratio and at the same combustion efficiency. At $CR_i = 2.04$ and $CR_i = 1.74$ conditions, airflow rates were estimated to be 0.23 and 0.27 kg $\cdot$ s^{-1},

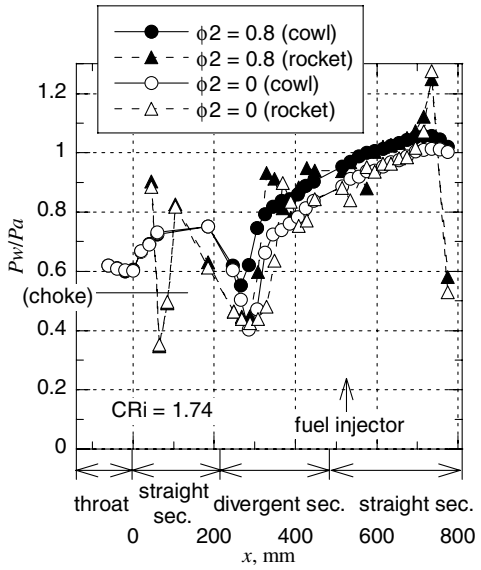

Fig. 7 Wall pressure distributions at $CR_i = 1.74$.

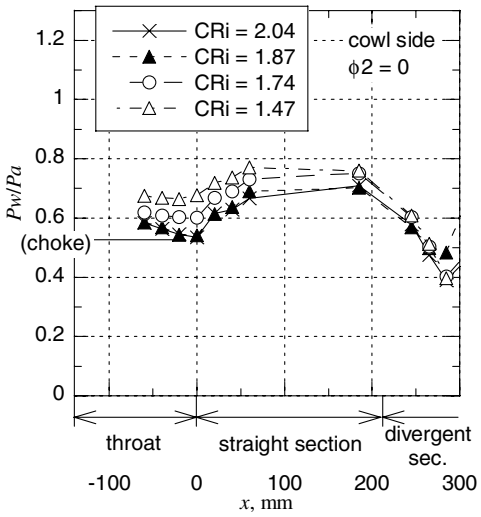

Fig. 8 Wall pressure distributions in throat section at $\phi 2 = 0$ condition.

respectively, even though choking was unattainable at the $CR_i = 1.74$ condition. However, pressure levels in the downstream straight section were similar in the two CR conditions.

The reason is discussed here. The mass flow rate is expressed as follows:

$$\dot{m} = PA \cdot M\sqrt{\frac{\gamma}{RT}} \tag{1}$$

Then,

$$P = \frac{1}{A}\frac{\dot{m}}{M}\sqrt{\frac{R \cdot T_t}{\gamma}}\frac{1}{\sqrt{1 + [(\gamma - 1)/2]M^2}} \tag{2}$$

The Mach number of the combustion gas in the downstream straight section is determined with the ratio of the area of the downstream section to that of the exit throat. Thus, pressure in the downstream straight section should increase with an increase of the mass flow rate. In spite of the increase of the breathed air, pressure in the downstream straight section hardly increased at the $CR_i = 1.74$ condition. This might have been caused by poor combustion efficiency of the fuel injected into the downstream straight section.

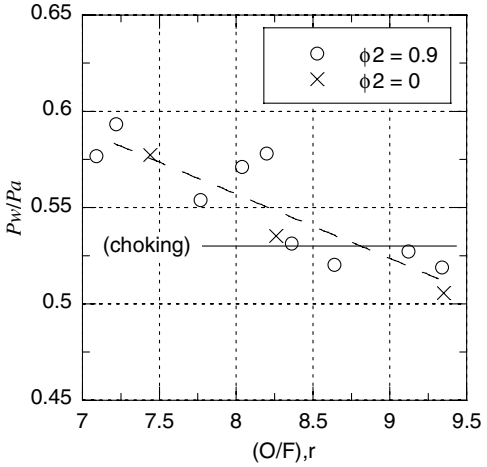

Fig. 9 Effect of rocket mixture ratio on suction of air.

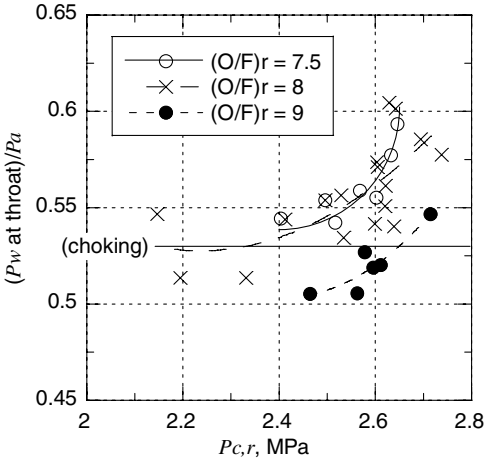

Fig. 10 Effect of rocket chamber pressure on suction of air.

Though the pressure in the throat section became lower with the increase of CR_i, the amount of breathed air increased with the decrease of CR_i. A larger amount of air causes larger thrust. When the choking of the breathed air is attained around the entrance of the divergent section and the pressure increase due to combustion in the downstream straight section does not propagate into the upstream straight section, a smaller CR_i is preferable to an increase of the rate of breathed airflow.

D. Rocket Operating Conditions

Figure 9 shows the effect of the rocket mixture ratio $(O/F)_r$ on suction performance. The rocket chamber pressure was 2.6 MPa, and $\phi 2 = 0.9$ or 0 in the baseline design condition. $\phi 2$ did not affect the suction performance because the influence of combustion in the downstream straight section did not propagate into the upstream straight section. One of the reasons for the scatter of the values was variance of rocket chamber pressure. The suction performance increased with the increase of the mixture ratio, that is, with heavier mean molecular weight.

The effect of rocket chamber pressure on suction performance was investigated at several rocket mixture ratios. Figure 10 shows wall pressure at $x = 0$ on the cowl side against the rocket chamber pressures. When the rocket chamber pressure increased, suction performance was degraded and choking unattainable. Although the impulse function increases with the increase of the chamber pressure, the suction performance is degraded. As the rocket chamber pressure increases, the pressure in the upstream straight section increases after the interaction between the rocket exhaust and the breathed air. It is difficult for the air choked at the throat section to expand in the

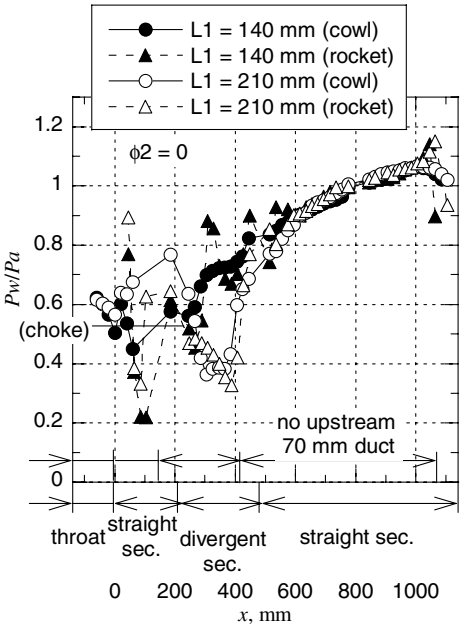

Fig. 11 Effect of length of upstream straight section on suction of air.

upstream straight section. Furthermore, the impulse function and the velocity of the air after the interaction decrease due to the higher pressure level in the interaction. With an increase of the rocket chamber pressure, it is difficult for the Mach number of the breathed air to increase after the interaction, and finally choking of the air is unattainable. According to the prediction by calculation in the design process, choking of the breathed air was unattainable at $P_{c,r} =$ 3.1 MPa and $(O/F)r = 8$.

E. Length of Upstream Straight Section

The effect of the length of the upstream straight section on the flow condition of the air was investigated. Figure 11 shows wall pressure distributions with the 140 mm and the 210 mm upstream straight sections. Figure 4 shows the model configuration with the 210 mm upstream straight section. By removing the hatched component in Fig. 4, the model configuration with the 140 mm section was attained. The condition of $\phi 2 = 0$ and the long downstream straight section were applied. With the 140 mm section, the pressure level in the upstream straight section was lower than that with the 210 mm section. With the 140 mm section, a pressure drop was not observed around the entrance of the divergent section on the cowl side, whereas with the 210 mm section, a clear decrease in pressure was measured there.

F. Exit Throat Area

The effect of the height at the exit throat on the flow conditions of gases was investigated. As CR_e increases, the Mach number becomes smaller and pressure becomes higher in the downstream straight section under the choking condition. Wall pressure distributions are shown in Fig. 12. As CR_e increases, the Mach number decreases and the impulse function increases upstream of the convergent section, that is, in the downstream straight section.

To realize the larger impulse function, the reaction force should increase in the divergent section. The pressure level obtained with a larger exit contraction ratio condition was higher in the divergent section and the starting position of the pseudoshock moved upstream. This higher pressure affected the interaction between the breathed air and the rocket exhaust in the upstream straight section, and made choking unattainable in the throat section at the $CR_e =$ 1.21 condition.

G. Equivalence Ratio

The effect of $\phi 2$ was investigated. Wall pressure distributions at various $\phi 2$ are shown in Fig. 13. The impulse function is expressed as follows:

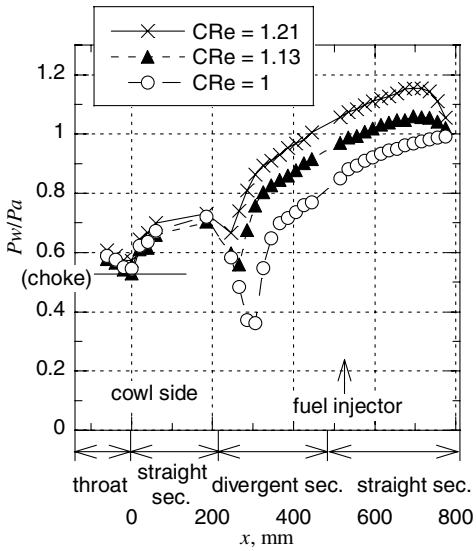

Fig. 12 Effect of exit throat height on wall pressure distribution.

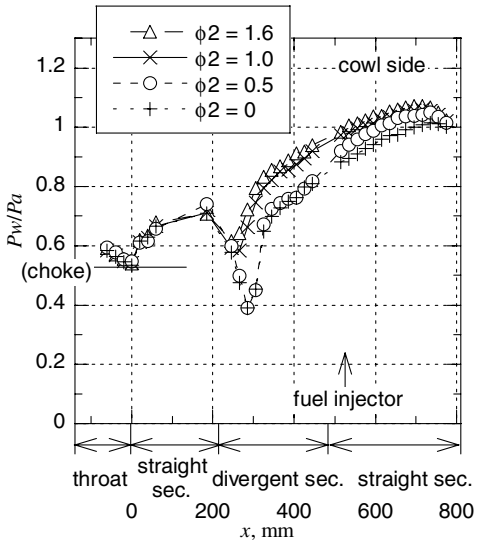

Fig. 13 Effect of equivalence ratio $\phi 2$ on wall pressure distribution.

$$F = \dot{m}u + PA = \dot{m}\frac{\sqrt{\gamma \cdot R \cdot T_t}}{\sqrt{1 + [(\gamma - 1)/2]M^2}}\left(M + \frac{1}{\gamma \cdot M}\right) \qquad (3)$$

The impulse function of combustion gas increases with an increase of total temperature, that is, an increase of the equivalence ratio.

As shown in Fig. 13, the pressure level in the divergent and downstream straight sections increased with the equivalence ratio. With the increase of $\phi 2$ from 0 to 0.5, the wall pressure became higher in the downstream straight section. With the further increase of $\phi 2$ from 0.5 to 1.0, the starting position of the pseudoshock moved upstream in the divergent section. When $\phi 2$ increased from 1.0 to 1.6, heat release did not increase greatly, and the increase of pressure in the divergent section was small.

H. Length of Downstream Straight Section and Fuel Injection Position

Figure 14 shows wall pressure distributions with the longer downstream straight section. Fuel injection positions are indicated in Fig. 4. The mixture ratio of the rocket $(O/F)_r$ was 7.8, slightly lower than 8. Thus, the suction performance was lower than in the baseline design condition, as shown in Fig. 9, and choking was broken at the throat.

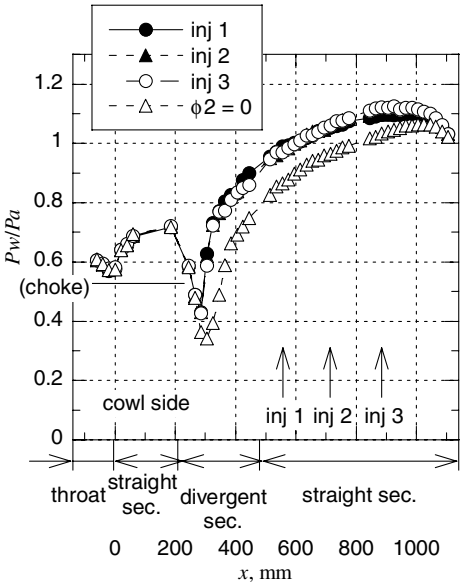

Fig. 14 Effects of length of downstream combustor and fuel injection location on wall pressure distributions.

Wall pressure distributions were similar, namely, no difference was attained by the fuel injection position in the downstream straight section. Furthermore, the starting position of the pseudoshock and the pressure level in the downstream straight section were similar to those in the baseline design condition with a shorter downstream straight section. The combustion condition was not improved with an increase in the length of the combustor.

IV. Conclusions

A combined-cycle combustor model was tested in the ejector-jet mode at a sea-level still condition. The following points were clarified.

1) Operation of the ejector-jet mode was demonstrated. That is, air was breathed and choked at the throat section. Rocket exhaust and air became supersonic around the entrance of the divergent section. Supersonic gases were decelerated to subsonic speed in the region of the pseudoshock in the divergent section. The subsonic mixture was accelerated to sonic speed by combustion and convergence of the combustor wall.

2) The experimental operating conditions reasonably well agreed with the predicted design conditions.

3) The mean Mach number was 1.0, and the mean combustion efficiency was 0.8 as shown by the pitot pressure measurement and gas sampling.

4) Several design factors were investigated. Area ratios affected suction performance at the entrance and pressure level at the exit. The mixture ratio and the chamber pressure of the rockets affected the suction performance of air. The length of the upstream straight section affected the pressure level in this section. The combustion status was not affected by the length of the downstream straight section or the position of fuel injection.

Acknowledgment

The authors wish to thank Sadatake Tomioka of the Japan Aerospace Exploration Agency for useful advice on the design of the experimental model.

References

[1] Escher, W. J. D., "A User's Primer for Comparative Assessments of All-Rocket and Rocket-Based Combined-Cycle Propulsion Systems for Advanced Earth-to-Orbit Space Transport Applications," AIAA Paper 95-2474, July 1995.

[2] Olds, J. R., and Bradford, J. E., "SCCREAM: A Conceptual Rocket-Based Combined-Cycle Engine Performance Analysis Tool," *Journal of Propulsion and Power*, Vol. 17, No. 2, 2001, pp. 333–339.

[3] Siebenhaar, A., "Strutjet Evolves to Meet Air-Breathing Propulsion Challenges for the 21st Century," 13th International Symposium on Air-Breathing Engines Paper ISABE 97-7135, Sept. 1997.

[4] Lee, J., and Krivanek, T., "Design and Fabrication of the ISTAR Direct-Connect Combustor Experiment at the NASA Hypersonic Tunnel Facility," AIAA Paper 2005-0611, Jan. 2005.

[5] Kanda, T., and Kudo, K., "Conceptual Study of a Combined-Cycle Engine for an Aerospace Plane," *Journal of Propulsion and Power*, Vol. 19, No. 5, 2003, pp. 859–867.

[6] Kanda, T., Tani, K., and Kudo, K., "Conceptual Study of a Rocket-Ramjet Combined-Cycle Engine for an Aerospace Plane," *Journal of Propulsion and Power*, Vol. 23, No. 2, 2007, pp. 301–309. doi:10.2514/1.22899

[7] Kubota, S., Masuya, G., and Tani, K., "Aerodynamic Performances of the Combined Cycle Inlet," International Council of the Aeronautical Sciences Paper 2004-6.6.1, Sept. 2004.

[8] Tani, K., Kanda, T., Kato, K., Sakuranaka, N., and Watanabe, S., "Designing and Aerodynamic Performance of the Combined Cycle Engine in a Hypersonic Flow," International Astronautical Congress (IAC) Paper 05-C4.5.06, Oct. 2005.

[9] Kanda, T., and Tani, K., "Momentum Balance Model of Flow Field with Pseudo-Shock," AIAA Paper 2005-1045, Jan. 2005.

[10] Kanda, T., Chinzei, N., Kudo, K., and Murakami, A., "Dual-Mode Operation in a Scramjet Combustor," *Journal of Propulsion and Power*, Vol. 20, No. 4, 2004, pp. 760–763.

[11] Kato, K., Kanda, T., Kobayashi, K., Kudo, K., and Murakami, A., "Downstream Ramjet-Mode Combustion in a Dual-Mode Scramjet Engine," *Journal of Propulsion and Power*, Vol. 22, No. 3, 2006, pp. 511–517.

[12] Kato, K., Kanda, T., Kudo, K., and Murakami, A., "Mach-8 Tests of a Combined-Cycle Engine Combustor," *Journal of Propulsion and Power* (to be published).

[13] Aoki, S., Lee, J., Masuya, G., Kanda, T., and Kudo, K., "Aerodynamic Experiment on an Ejector-Jet," *Journal of Propulsion and Power*, Vol. 21, No. 3, 2005, pp. 496–503.

[14] Tani, K., Kanda, T., and Tokudome, S., "Aerodynamic Characteristics of the Combined Cycle Engine in an Ejector Jet Mode," AIAA Paper 2005-1210, Jan. 2005.

[15] Tani, K., Kanda, T., and Tokudome, S., "Aerodynamic Characteristics of the Modified Combined Cycle Engine in Ejector-Jet Mode," AIAA Paper AIAA-2006-0224, Jan. 2006.

[16] Bartz, D. R., "A Simple Equation for Rapid Estimation of Rocket Nozzle Convective Heat Transfer Coefficients," *Jet Propulsion*, Vol. 27, No. 1, 1957, pp. 49–51.

[17] Niino, M., Kumakawa, A., Yatsuyanagi, N., Gomi, H., Suzuki, A., Sakamoto, H., Sasaki, M., and Yanagawa, K., "A Study on Heat Transfer Characteristics of Water Cooled LO2/LH2 Rocket Combustor," Technical Report of National Aerospace Laboratory, NAL TR-708, May 1982 (in Japanese).

[18] Mitani, T., Takahashi, M., Tomioka, S., Hiraiwa, T., and Tani, K., "Analyses and Application of Gas Sampling to Scramjet Engine Testing," *Journal of Propulsion and Power*, Vol. 15, No. 4, 1999, pp. 572–577.

[19] Chapman, D. R., Kuehn, D. M., and Larson, H. K., "Investigation of Separated Flows in Supersonic and Subsonic Streams with Emphasis on the Effect of Transition," NACA Rept. TR-1356, 1958.

[20] Schmucker, R. H., "Status of Flow Separation Prediction in Liquid Propellant Rocket Nozzles," NASA TM X-64890, Nov. 1974.

[21] Mager, A., "On the Model of the Free, Shock-Separated, Turbulent Boundary Layer," *Journal of the Aeronautical Sciences*, Vol. 23, No. 2, Feb. 1956, pp. 181–184.

[22] Korkegi, R. H., "Comparison of Shock-Induced Two- and Three-Dimensional Incipient Turbulent Separation," *AIAA Journal*, Vol. 13, No. 4, 1975, pp. 534–535.

T. Wang
Associate Editor